Radiation Physics and Chemistry 199 (2022) 110363

Contents lists available at ScienceDirect

Radiation Physics and Chemistry

journal homepage: www.elsevier.com/locate/radphyschem

A model for Geant4-DNA to simulate ionization and excitation of liquid water by protons travelling above 100 MeV

A.D. Domínguez-Muñoz [a,*], M.I. Gallardo [a], M.C. Bordage [b], Z. Francis [c], S. Incerti [d], M.A. Cortés-Giraldo [a,**]

[a] Department of Atomic, Molecular and Nuclear Physics, Universidad de Sevilla, Seville, Spain
[b] Université Toulouse III-Paul Sabatier, UMR1037 CRCT, Toulouse, France
[c] Department of Physics, Faculty of Sciences, Université Saint Joseph, Beirut, Lebanon
[d] University of Bordeaux, CENBG, UMR 5797, F-33170, Gradignan, France

ARTICLE INFO

Keywords:
Proton
Liquid water
Geant4-DNA
RPWBA
Dielectric function
Ionization and excitation

ABSTRACT

Biological damage induced by ionizing radiation plays a major role in many application fields as radiotherapy and microdosimetry. Geant4-DNA Monte Carlo track-structure code has the capability to simulate the passage of radiation through liquid water, containing physical, physicochemical and chemical processes that lead the early DNA damage. For proton projectile, current models reach up to an incident energy of 100 MeV. In order to cover the entire energy regime involved in proton radiotherapy, this work presents a new model that extends proton ionization and excitation of liquid water up to 300 MeV. Calculation of cross section dataset is made for ionization of five ionization shells and five excitation levels of liquid water using the Relativistic Plane Wave Born Approximation (RPWBA). Implementation is validated through the *spower* and *range* examples of the official release, obtaining an agreement within 1% with respect to reference data published in ICRU90 report.

1. Introduction

Track structure calculations of radiation traversing biological medium are widely employed in many radiation research fields such as radiotherapy, radiobiology and microdosimetry (Perales et al., 2019; Bertolet et al., 2019a, 2019b), among others. It is possible to model the energy deposition together with physical and chemical processes at sub-cellular scale which induce later damage to DNA. Great efforts have been made to model interactions of radiation with liquid water, which is the main component of soft tissue. In case of proton radiotherapy, it is important to calculate proton dose distribution at microscopic scale for the entire track in order to calculate biological effect not only in tumour but also in healthy surrounding tissue to study possible secondary side effects resulting from treatment.

The Geant4-DNA package (Incerti et al., 2010a, 2010b, 2018; Bernal et al., 2015), an extension of the Geant4 Monte Carlo toolkit dedicated to modelling biological damage at DNA scale by different incident particles, is one of the most popular codes available for this purpose. As the DNA damage can be caused either by direct interaction of the incident particles (direct damage) or by reactions with radiation-induced radicals created in water (indirect damage), Geant4-DNA contains physics processes as well as physico-chemistry and chemistry processes for water radiolysis. On the one hand, this package handles radiation-matter physical interactions using different physics processes (such as ionization or excitation), being each described by one or more interaction models depending on the projectile type and energy. Such interaction models need to be accurate because of the direct impact over initial radiolysis products which are generated during the physical–chemical stage (Shin et al., 2021). On the other hand, several studies were carried out to improve the simulation of chemical stage as estimation of track segment yields of water radiolysis species around the Bragg peak energy region (Baba et al., 2021a), and assess the influence of multiple ionization processes of liquid water on the radiation chemical yields values (Baba et al., 2021b). Furthermore, other works have been focused on the modelling of the mechanisms of DNA damage induction in order to calculate single and double strand breaks in more complex DNA geometries as found in human cells (Sakata et al., 2019).

Proton interaction processes with liquid water are usually modelled

* Corresponding author.
** Corresponding author.
E-mail addresses: ad.dominguezmunoz@gmail.com (A.D. Domínguez-Muñoz), miancortes@us.es (M.A. Cortés-Giraldo).

https://doi.org/10.1016/j.radphyschem.2022.110363
Received 1 February 2022; Received in revised form 25 May 2022; Accepted 21 June 2022
Available online 2 July 2022
0969-806X/© 2022 The Authors. Published by Elsevier Ltd. This is an open access article under the CC BY-NC-ND license (http://creativecommons.org/licenses/by-nc-nd/4.0/).

considering (Dingfelder et al., 2000) five ionized molecular states, five excited molecular states and electron capture. Thus, in order to simulate a proton beam it is also necessary to take into account interaction processes of neutral hydrogen with liquid water. However current models can be used up to an incident energy of 100 MeV (Incerti et al., 2010b) while therapeutic proton beams can reach 270 MeV (Paganetti, 2016). Thus, only protons beams of up to roughly 7 cm range can be simulated with current Geant4-DNA models. In case of ionization and excitation, the Born model is employed to simulate incident protons from 500 keV to 100 MeV. This model applies the First Born Approximation together with the Bethe theory to obtain a non-relativistic expression for doubly-differential cross section in energy transfer and momentum transfer (Dingfelder et al., 2000). For incident energies comparable to proton rest energy, the Bethe differential cross section is corrected to include relativistic effects and transverse interaction.

The aim of this work is to develop a new Geant4-DNA model class for proton interaction with liquid water above 100 MeV incident energy. For this energy regime, electron capture cross section is several orders of magnitude lower than ionization and excitation. Thus in order to extend the current upper limit of Geant4-DNA, we focused on ionization and excitation processes only. The new model is an interpolated type model, which means that it reads previously generated data-tables of single differential cross section (DCS) in projectile energy loss and total cross section (CS) for the five ionization shells and the five excitation transitions separately. The DCS and CS datasets were produced with a model based on Relativistic Plane Wave Born Approximation (RPWBA) and Generalized Oscillator Strength (GOS) describing target response (Salvat, 2013; Dingfelder et al., 2000; Emfietzoglou et al., 2017; Scifoni et al., 2010). We started from the doubly-differential cross section (DDCS) expression given by the RPWBA theory which is applicable for relativistic energies and also incorporate both longitudinal and transverse interaction, without any correction needed subsequently. Detailed explanation of the RPWBA theory, the GOS used in this work for liquid water, and the Fermi density effect is presented in section 2. The new upper limit was established at 300 MeV, enough to cover the entire range of proton therapy clinical beams and to ensure that secondary electrons have kinetic energy lower than 1 MeV, which is the current upper limit for electron transport in Geant4-DNA. Section 3 contains the comparison of CS values of this work with current models available in Geant4-DNA below 100 MeV and implementation verification by calculation of stopping power and range above 100 MeV. Finally, conclusions are drawn in section 4.

2. Materials and methods

2.1. Differential and total cross-section

The initial state of the proton (projectile), just before the collision, is characterized by its incident kinetic energy E and momentum $\mathbf{p}$, both in laboratory frame in which the water molecule (target) is assumed to be at rest. After the collision, the kinetic energy and momentum of the proton are denoted by E' and $\mathbf{p}'$, respectively. The inelastic interaction of a proton with a single electron of a water molecule is described in terms of energy loss by the projectile $W \equiv E - E'$ and momentum transfer $\mathbf{q} \equiv \mathbf{p} - \mathbf{p}'$. For the case of ionization and excitation, the energy loss by the proton is equal to the energy transfer to the electron $W \equiv \varepsilon' - \varepsilon$, where ε and ε' are, respectively, the initial and final energies of the electron in the process.

Water, in liquid phase, was modelled as a homogeneous isotropic medium. We assumed that the collision depends only on the magnitude of the momentum transfer $q \equiv |\mathbf{q}|$, which is given by

$$q^2 = p^2 + p'^2 - 2pp'\cos\theta, \tag{1}$$

where c is the speed of light in vacuum, p and p' are the magnitudes of $\mathbf{p}$ and $\mathbf{p}'$, respectively, and θ is the scattering angle or the angle between initial and final momentum. Instead of using q, it is more convenient to work with the so-called recoil energy Q which is the kinetic energy of a free electron with momentum $\mathbf{q}$. Mathematically

$$Q(Q + 2m_e c^2) = (qc)^2, \tag{2}$$

being m_e the electron rest mass and c the speed of light.

The recoil energy Q is closely related to the energy transfer W as it represents the recoil of a molecular electron after the collision (Fano, 1963). When the energy transfer is much smaller than the incident energy of the projectile ($W \ll E$), the recoil energy Q depends only on the scattering angle. Conversely, in the limit of large q, when molecular electrons can be considered free and at rest, Q becomes equal to W.

2.1.1. RPWBA theory

The doubly-differential cross section (DDCS) in W and Q of individual collision of a proton projectile with a bound electron of an atom or molecule, $\mathrm{d}^2\sigma/\mathrm{d}W\mathrm{d}Q$, in the Relativistic Plane Wave Born Approximation (RPWBA) (Fano, 1963; Inokuti, 1971) can be written, as stated in (Salvat, 2013), as follows:

$$\frac{\mathrm{d}^2\sigma}{\mathrm{d}W\mathrm{d}Q} = \frac{2\pi k_e^2 e^4}{m_e c^2 \beta^2}\left\{\frac{2m_e c^2}{WQ(Q+2m_e c^2)} + \frac{2m_e c^2 W}{\left[Q(Q+2m_e c^2) - W^2\right]^2}\left[\beta^2 - \frac{W^2}{Q(Q+2m_e c^2)}\right]\right\}\frac{\mathrm{d}f(Q,W)}{\mathrm{d}W}, \tag{3}$$

where k_e is the Coulomb constant, e is the elementary electron charge and β the proton incident velocity in units of c. The factor $\mathrm{d}f(Q, W)/\mathrm{d}W$ is the atomic/molecular generalized oscillator strength (GOS) that characterizes the response of the atomic/molecular target electron to the interaction with the projectile, containing the sum over all initial and final states of the target in the matrix element of the interaction hamiltonian once the integration over the space coordinates of the projectile is done. As it can be seen, the DDCS only depends on the charge and the velocity of projectile, but not on its mass.

RPWBA theory treats the interaction of the projectile with the molecular electron as a first-order perturbation (Born approximation), which is fully applicable for the energy range involved in this work. The interaction contains two terms. The first one, the longitudinal term, accounts for the unretarded Coulomb interaction between the projectile and the target. The second one contains the transverse term or exchange of virtual photons. Both of them correspond to the two terms inside the braces in eq. (3), respectively. Initial and final projectile states are described as free states; in other words, initial and final projectile wavefunctions are relativistic plane waves. The plane-wave approximation allows the separation of projectile and target contributions to the DDCS.

The single differential cross section (DCS) in W is obtained integrating the DDCS in Q, i.e.

$$\frac{\mathrm{d}\sigma}{\mathrm{d}W} = \int_{Q_-(W)}^{Q_+(W)} \frac{\mathrm{d}^2\sigma}{\mathrm{d}W\mathrm{d}Q}\,\mathrm{d}Q, \tag{4}$$

where the limits of integration $Q_\pm$ are given by eqs. (1) and (2) considering $\cos\theta = \pm 1$. Corresponding values for proton projectile with different incident energies E are shown in Fig. 1.

The calculation of cross section (CS) is obtained by

$$\sigma = \int_0^E \frac{\mathrm{d}\sigma}{\mathrm{d}W}\,\mathrm{d}W. \tag{5}$$

In order to compare with experimental data, it is useful to introduce the computation of the electronic stopping power or energy loss per unit path length

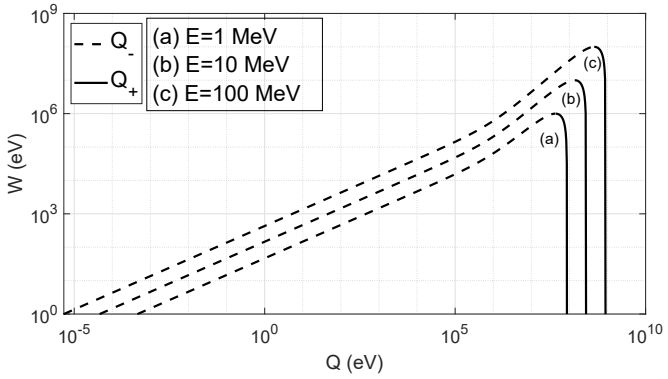

Fig. 1. Kinematic integration limits of recoil energy $Q_{\pm}$ as function of projectile energy loss W for different incident energies E for a proton projectile.

$$\mathcal{S} = \mathcal{N}\int_0^E W\frac{\mathrm{d}\sigma}{\mathrm{d}W}\,\mathrm{d}W, \tag{6}$$

where $\mathcal{N}$ is the number of atoms/molecules per unit volume of the medium.

2.1.2. Collision in dense medium, the Fermi density effect

Equation (3) for the DDCS is strictly correct for the interaction of the projectile with isolated atoms/molecules. When the incident particle is passing through a condensed medium with dielectric properties, it induces the polarization of the surrounding atoms/molecules, which impacts the transverse interaction; this is the well known Fermi density effect (Fermi, 1940; Inokuti and Smith, 1982; Sternheimer et al., 1982). This effect is only significant at proton energies above few hundred MeV and it produces a reduction of the stopping power $\mathcal{S}$ obtained from DDCS eq. (3). The correction is expected to be of few percent in the case of solids and liquids and, of course, it vanishes for low-density medium.

When the medium is in condensed phase, aggregation effects have to be taken into account in initial and final atomic/molecular states of target electron that constitute the GOS in eq. (3). In other words, surrounding atoms/molecules perturb the electronic states, the outer shells (those with less bound energy) being the most affected by this issue.

Using the dielectric stopping theory of charged particles in dense media (Jackson and Fox, 1999) and following the approach suggested by Fernández-Varea (Fern á ndez-Varea et al., 2005), it is possible to obtain a correction to the RPWBA theory corresponding to the Fermi density effect. We define the Fermi correction to the cross section $\Delta\sigma_F$, so that the cross section with Fermi density effect included, σ_F, is obtained from

$$\sigma_F = \sigma + \Delta\sigma_F. \tag{7}$$

The Fermi density effect correction to the DDCS eq. (3) is thus expressed with the formula

$$\frac{\mathrm{d}^2\Delta\sigma_F}{\mathrm{d}W\mathrm{d}Q} = \frac{2\pi k_e^2 e^4}{m_e c^2\beta^2}\left\{\mathrm{Im}\left(\frac{1}{Q(Q+2m_ec^2)-W^2\varepsilon(Q,W)}\right)\frac{|\varepsilon(Q,W)|^2}{\mathrm{Im}(\varepsilon(Q,W))} - \frac{2m_ec^2W}{\left[Q(Q+2m_ec^2)-W^2\right]^2}\right\}\left[\beta^2-\frac{W^2}{Q(Q+2m_ec^2)}\right]\frac{\mathrm{d}f(Q,W)}{\mathrm{d}W}, \tag{8}$$

where $\varepsilon(Q, W)$ is the dielectric function (DF) of the medium and $\mathrm{Im}(\cdot)$ denotes the imaginary part of the argument. The GOS $\frac{\mathrm{d}f(Q,W)}{\mathrm{d}W}$ is defined in terms of the DF by

$$\frac{\mathrm{d}f(Q,W)}{\mathrm{d}W} \equiv W\left(1+\frac{Q}{m_ec^2}\right)\frac{2Z}{\pi\Omega_p^2}\,\mathrm{Im}\left(\frac{-1}{\varepsilon(Q,W)}\right), \tag{9}$$

where Z is the number of electrons in one atom/molecule of the medium and Ω_p is the plasma resonance energy of an electron gas with number of electrons per unit of volume equivalent to that of the stopping medium $\mathcal{N}Z$, defined as

$$\Omega_p^2 = 4\pi\mathcal{N}Z\hbar^2e^2\big/m_e, \tag{10}$$

where $\hbar$ is the reduced Planck constant.

The expression of stopping power in dielectric theory is obtained by writing the electromagnetic field, induced by the charged projectile in the medium, in terms of the dielectric function $\varepsilon(\mathbf{k}, \omega)$ expressed as a function of the wave vector $\mathbf{k}$ and the frequency ω corresponding to the Fourier transform of the components of the electromagnetic field. Again, for an isotropic homogeneous medium the DF depends only on the wavenumber $|\mathbf{k}| = k$. In general, $\varepsilon(k, \omega)$ is a complex function which contains the information of polarization and energy absorption of the medium resulting from the action of an electromagnetic field. The correspondence between classical dielectric theory and quantum theory is made assuming the semi-classical relationships $q = \hbar k$ and $W = \hbar\omega$.

The contribution of the density effect to DCS, CS and stopping power is calculated analogously to the quantum case, i.e.

$$\frac{\mathrm{d}\Delta\sigma_F}{\mathrm{d}W} = \int_{Q_-(W)}^{Q_+(W)}\frac{\mathrm{d}^2\Delta\sigma_F}{\mathrm{d}W\mathrm{d}Q}\,\mathrm{d}Q, \tag{11}$$

$$\Delta\sigma_F = \int_0^E\frac{\mathrm{d}\Delta\sigma_F}{\mathrm{d}W}\,\mathrm{d}W, \tag{12}$$

$$\mathcal{S}_{\Delta\sigma_F} = \mathcal{N}\int_0^E W\frac{\mathrm{d}\Delta\sigma_F}{\mathrm{d}W}\,\mathrm{d}W. \tag{13}$$

2.2. Dielectric function and GOS of liquid water

Obtaining the GOS of liquid water from interaction matrix elements is a complicated procedure due to the molecular geometry, without spherical symmetry, and aggregation effects mentioned above; the latter is applicable to any molecular dense medium. Then, the dielectric function plays an important role in GOS computation, as shown in eq. (9), which is essential in RPWBA theory of energy loss. Especially, the GOS depends on the energy-loss function (ELF) η_2

$$\eta_2(Q,W) \equiv \mathrm{Im}\left(\frac{-1}{\varepsilon(Q,W)}\right) = \frac{\varepsilon_2(Q,W)}{\varepsilon_1^2(Q,W)+\varepsilon_2^2(Q,W)}, \tag{14}$$

obtained by decomposition of the complex DF in its real and imaginary parts, respectively, denoted ε_1 and ε_2: $\varepsilon = \varepsilon_1 + i\varepsilon_2$. Both parts satisfy the Kramers-Kronig relationship (Landau et al., 1961)

$$\varepsilon_1(Q,W) = 1+\frac{1}{\pi}\mathcal{P}\left[\int_{-\infty}^{+\infty}\frac{\varepsilon_2(Q,W')}{W'-W}\,\mathrm{d}W'\right], \tag{15}$$

$$\varepsilon_2(Q,W) = -\frac{1}{\pi}\mathcal{P}\left[\int_{-\infty}^{+\infty}\frac{\varepsilon_1(Q,W')-1}{W'-W}\,\mathrm{d}W'\right], \tag{16}$$

where $\mathcal{P}[\cdot]$ stands for Cauchy principal value. In eq. (14), the numerator accounts for characteristic photoabsorption spectrum that sets off single-electron transition and the denominator represent the long-range polarization and screening effect of the medium (Emfietzoglou et al., 2005). In low-density medium, $\varepsilon_1 \simeq 1$ and $\varepsilon_2 \ll 1$, thus the effect of the denominator vanishes and $\eta_2 \simeq \varepsilon_2$.

Following previous works (Dingfelder et al., 1999; Emfietzoglou et al., 2005), we have considered five ionization shells ($1b_1$, $3a_1$, $1b_2$, $2a_1$, and the K-shell of oxygen) and five excitation states (A^1B_1, B^1A_1, Ryd A + B, Ryd C + D, and diffuse bands) of the water molecule. In case of ionization, a distinction was made between inner shell (K-shell of oxygen) and outer shells (valence bands). The imaginary part of the liquid water DF was thus decomposed in terms as follows

$$\varepsilon_2(Q,W) = \varepsilon_{2,\mathrm{K}}(Q,W) + \sum\nolimits_{j_i}^{\mathrm{ion}}\varepsilon_{2,j_i}(Q,W) + \sum\nolimits_{j_e}^{\mathrm{exc}}\varepsilon_{2,j_e}(Q,W), \tag{17}$$

with $\varepsilon_{2,\mathrm{K}}$ corresponding to oxygen K-shell ionization, ε_{2,j_i} corresponding to outer shells ionization and ε_{2,j_e} corresponding to excitation states. The ELF for a specific excitation level or ionization process j, $\eta_{2,j}$, is obtained according to

$$\eta_{2,j}(Q,W) = \frac{\varepsilon_{2,j}(Q,W)}{\varepsilon_1^2(Q,W)+\varepsilon_2^2(Q,W)}. \tag{18}$$

This allows the separate calculation of the contribution of each excitation state and ionization shell to the DDCS.

The unprocessed imaginary part of the DF for ionization/excitation, $\varepsilon_{2,j_i/j_e}^{(\mathrm{un})}$, was computed with the formula

$$\varepsilon_{2,j_i/j_e}^{(\mathrm{un})}(Q,W) = \Omega_p^2\, D_{j_i/j_e}(Q,W), \tag{19}$$

where $D_{j_i/j_e}(Q,W)$ are the extended-Drude functions calculated as indicated below.

For ionization, ε_{2,j_i} was determined using a semi-empirical model based on extended-Drude functions

$$D_{j_i}(Q,W) = f_{j_i}(Q)\,\frac{\gamma_{j_i}(Q)\,W}{\left(U_{j_i}^2(Q)-W^2\right)^2+\gamma_{j_i}^2(Q)\,W^2}, \tag{20}$$

while for excitation, ε_{2,j_e} was obtained with extended derivative-Drude functions

$$D_{j_e}(Q,W) = f_{j_e}(Q)\,\frac{2\gamma_{j_e}^3(Q)\,W^3}{\left[\left(U_{j_e}^2-W^2\right)^2+\gamma_{j_e}^2(Q)\,W^2\right]^2}, \tag{21}$$

where $U_{j_i}(Q)$ and U_{j_e} are the transition energy coefficients, $f_{j_i/e}(Q)$ is the oscillator strength, and $\gamma_{j_i/e}(Q)$ is the damping energy. In the optical limit $Q=0$, eqs. (20) and (21) tend to Drude functions (Ritchie et al., 1991).

The value of the parameters in the optical limit were obtained by fitting experimental data to the sum of four $D_{j_i}(0,W)$ and five $D_{j_e}(0,W)$ functions for the entire range available in W (Emfietzoglou et al., 2005). The Q-dependence of coefficients as well as the values of parameters were taken from the ECN (Emfietzoglou-Cucinotta-Nikjoo) model proposed by Emfietzoglou et al. (2005). The extended-Drude functions $D_{j_i}(Q,W)$ have non-zero values below the binding energy threshold. Thus, in case of ionization, a post-processing method of truncation, smoothing and redistribution was needed (Emfietzoglou et al., 2017). In excitation case, we must point out that eq. (21) is sharply peaked at $W \approx U_{j_e}$, then it is more appropriate to describe the excitation as a discrete process rather than using eq. (20).

The only inner-shell, the oxygen K-shell, has large binding energy ($\sim$ 540 eV) as compared with outer shells. It is not affected by collective and aggregation effects and has a remarkable atomic behaviour. For high energy transfers, the real and imaginary parts of the DF are approximately $\varepsilon_1 \simeq 1$ and $\varepsilon_2 \ll 1$, thus the K-shell ELF can be approximated by $\eta_{2,K} \approx \varepsilon_{2,K}$ (Dingfelder et al., 2000). In this work, we have used the hydrogenic GOS approximation, which improves the asymptotic behaviour of Drude functions eq. (20) used earlier for outer shells (Emfietzoglou et al., 2009). An specific expression for oxygen K-shell GOS used can be found elsewhere (Heredia-Avalos et al., 2005).

With the aim of calculating $\varepsilon_1(Q,W)$, it is convenient to define the corresponding Kramers-Kronig function (Dingfelder et al., 1999) of the extended Drude function

$$D_{j_i}^{\mathrm{K-K}}(Q,W) \equiv \frac{1}{\pi}\mathcal{P}\left[\int_{-\infty}^{+\infty}\frac{D_{j_i}(Q,W')}{W'-W}\mathrm{d}W'\right] = f_{j_i}(Q)\,\frac{U_{j_i}^2(Q)-W^2}{\left[U_{j_i}^2(Q)-W^2\right]^2+\gamma_{j_i}^2(Q)\,W^2} \tag{22}$$

and of the extended derivative-Drude function

$$\begin{aligned} D_{j_e}^{\mathrm{K-K}}(Q,W) &\equiv \frac{1}{\pi}\mathcal{P}\left[\int_{-\infty}^{+\infty}\frac{D_{j_e}(Q,W')}{W'-W}dW'\right] \\ &= f_{j_e}(Q)\,\frac{\left(U_{j_e}^2-W^2\right)\left[\left(U_{j_e}^2-W^2\right)^2+3\gamma_{j_e}^2(Q)\,W^2\right]}{\left[\left(U_{j_e}^2-W^2\right)^2+\gamma_{j_e}^2(Q)\,W^2\right]^2}. \end{aligned} \tag{23}$$

The real part of the DF is therefore

$$\varepsilon_1(Q,W) = 1+\Omega_p^2\left[\sum_{j_i}D_{j_i}^{K-K}(Q,W)+\sum_{j_e}D_{j_e}^{K-K}(Q,W)\right]. \tag{24}$$

Fig. 2 shows the imaginary and real parts of the DF together with ELF for different Q values. These curves were obtained from eqs. (14), (17) and (24) using parameter values proposed by Emfietzoglou et al., 2005, 2017.

The post-processing method to get the DF for outer-shell ionization consisted of three steps. First, truncation of Drude functions below the binding energy shell B_{j_i} using Heaviside step function $\Theta(\cdot)$. Second, the smoothing just above the energy threshold via a gaussian type-function $S_{j_i}(W)$. Third and last, the truncated and smoothed parts of higher binding energy Drude function were redistributed among lower energy ionization levels with weights

$$w_{j_i j_i'}(Q,W) = \frac{D_{j_i}(Q,W)\,\Theta(W-B_{j_i})}{\sum_{j_i'':B_{j_i''}<B_{j_i'}}D_{j_i''}(Q,W)\,\Theta(W-B_{j_i''})}. \tag{25}$$

The imaginary part of outer-shell ionization DF was then calculated as follows

$$\begin{aligned} \varepsilon_{2,j_i}(Q,W) &= \varepsilon_{2,j_i}^{(\mathrm{un})}(Q,W)\left[1-S_{j_i}(W)\right]\Theta\left(W-B_{j_i}\right)+ \\ &+\sum_{j_i':B_{j_i}<B_{j_i'}}w_{j_i j_i'}(Q,W)\,\varepsilon_{2,j_i'}^{(\mathrm{un})}(Q,W)\times \\ &\times\left[\Theta\left(B_{j_i'}-W\right)+S_{j_i'}(W)\,\Theta\left(W-B_{j_i'}\right)\right]. \end{aligned} \tag{26}$$

Fig. 3a shows an example of the effect of post-processing for $Q=0$ (optical limit).The main aspects to highlight are the soft truncation below each binding energy and the redistribution only to lower binding energy shells according to their relative strength. The truncated part below the lowest binding energy, corresponding to $1b_1$ shell, will be treated as indicated hereafter.

In case of excitation, the imaginary part of the DF was obtained by

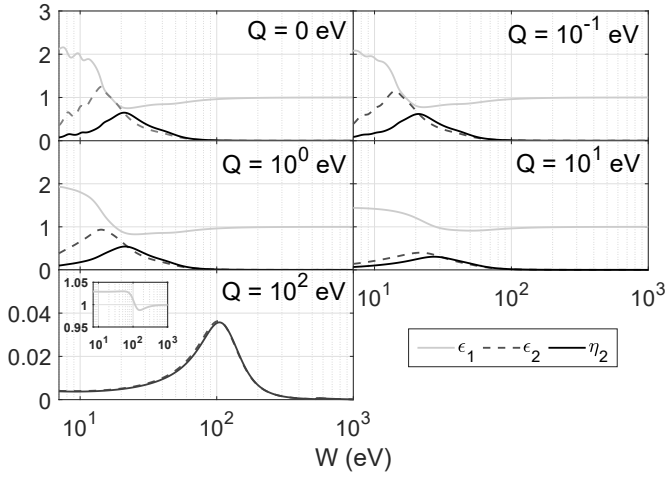

Fig. 2. Real and imaginary parts of the dielectric function (ε_1 and ε_2) and the energy loss function (η_2) of liquid water as function of projectile energy loss W for different values of recoil energy Q. The experimental cutoff energy is set to 7 eV.

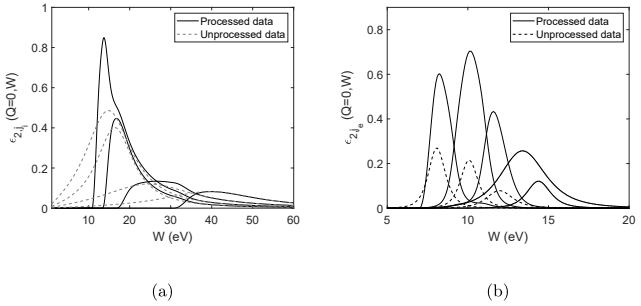

Fig. 3. (a) Processed (solid lines) and unprocessed (dotted lines) imaginary part of the dielectric function for ionization of outer shells of liquid water, $\varepsilon^{(un)}_{2,j_i}$ and ε_{2,j_i} respectively, at optical limit ($Q = 0$) in terms of projectile energy loss W. From left to right, lines correspond to $1b_1$, $3a_1$, $1b_2$ and $2a_1$ shells with ionization threshold energies $B_{j_i} = 10.79$, 13.40, 16.85 and 30.80 eV, respectively (Dingfelder, 2014). (b) Processed and unprocessed imaginary part of the dielectric function for excitation processes of liquid water, $\varepsilon^{(un)}_{2,j_e}$ and ε_{2,j_e} respectively, at optical limit ($Q = 0$) in terms of projectile energy loss W. From left to right, lines correspond to A^1B_1, B^1A_1, Ryd A + B, Ryd C + D and diffuse bands excitation transition. Note the lower cutoff at $W_{cut} = 7$ eV and that the two last levels are not processed because their excitation energy coefficients ($U_{\text{Ryd C + D}}$ and $U_{\text{diffuse bands}}$) are larger than the lower ionization threshold energy (B_{1b_1}).

means of eq. (21) and adding the smoothing of the Drude function with the lowest binding energy, the $1b_1$ shell, and the truncation of all ionization Drude functions below the lowest energy threshold B_{1b_1} analogously to the ionization case, only for transition with $j_e : U_{j_e} < B_{3a_1} = 13.40$ eV (value taken from (Dingfelder, 2014)). Thus

$$\varepsilon_{2,j_e}(Q,W) = \left\{\varepsilon^{(un)}_{2,j_e}(Q,W) + w_{j_e}(Q,W)\left[\sum_{j_i}\varepsilon^{(un)}_{2,j_i}(Q,W)\,\Theta\left(B_{1b_1} - W\right) + \right.\right.$$
$$\left.\left. + \varepsilon_{2,1b_1}(Q,W)\,S_{1b_1}(W)\,\Theta(W - B_{1b_1})\right]\right\}\times$$
$$\times\left[1 - S_{j_e}(W)\right]\Theta(W - W_{cut}), \tag{27}$$

where W_{cut} is the lowest energy cutoff for excitation set at 7 eV (Emfietzoglou et al., 2005), the weights were obtained from

$$w_{j_e}(Q,W) = \frac{D_{j_e}(Q,W)}{\sum\limits_{j'_e:U_{j'_e}<B_{3a_1}} D_{j'_e}(Q,W)}, \tag{28}$$

and $S_{j_e}(W)$ is a gaussian-type smoothing function.

After the post-processing, for $Q = 0$ case, the imaginary part remains as shown in Fig. 3b. Only the three lower excitation transitions (A^1B_1, B^1A_1 and Ryd A + B) are affected by the low energy interval redistribution of unprocessed DF imaginary part for ionization process. It is important to remark that the three excitation transitions affected by the distribution preserve the peaked shape of the derivative-Drude function eq. (21).

The GOS for each ionization shell df_{j_i}/dW was obtained from

$$\frac{df_{j_i}(Q,W)}{dW} \equiv W\left(1 + \frac{Q}{m_e c^2}\right)\frac{2Z}{\pi\Omega_p^2}\,\eta_{2,j_i}(Q,W), \tag{29}$$

$\eta_{2,j_i}(Q,W)$ being the ELF (eq. (18)) with the imaginary part of DF (eq. (26)). Fig. 4 displays the GOS for each ionization shell. Valence shells have a soft growth in direction of increasing W from binding threshold. In contrast, K-shell presents a sharp edge in W, typical of inner shells ionization which are not affected by phase effects.

As for the excitation cases, we took into consideration that "formally" excitation GOS is different from zero only for a discrete energy transfer value. Assuming a broadening in experimental peaks and

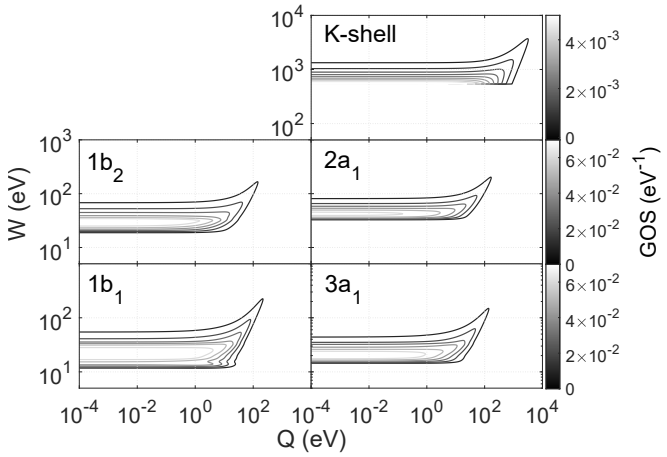

Fig. 4. Ionization GOS for different shells of the water molecule in condensed phase in terms of projectile energy loss W and recoil energy Q. Note that in case of the inner shell (K-shell of oxygen) the scale is one order of magnitude lower than those used for the outer shells.

bearing in mind that the GOS must fulfill the Bethe sum-rule (Dingfelder et al., 1999; Emfietzoglou et al., 2005), we obtained the excitation GOS df_{j_e}/dW from

$$\frac{df_{j_e}(Q,W)}{dW} = f_{j_e}(Q)\,\delta(W - W_{j_e}), \tag{30}$$

with

$$f_{j_e}(Q) \equiv \int_0^\infty W\left(1 + \frac{Q}{m_e c^2}\right)\frac{2Z}{\pi\Omega_p^2}\,\eta_{2,j_e}(Q,W)\,dW, \tag{31}$$

where $\eta_{2,j_e}(Q,W)$ is the ELF (18) with the imaginary part of DF (27). Results are presented in Fig. 5. Finally, the contribution of each process to the DDCS and Fermi correction was obtained by substituting the corresponding GOS in eqs. (3) and (8).

2.3. Integration into the Geant4-DNA package

The RPWBA model was included in Geant4-DNA model library following the design *G4VEmModel* (Incerti et al., 2010b). Then two new model classes, one for ionization and another for excitation, were

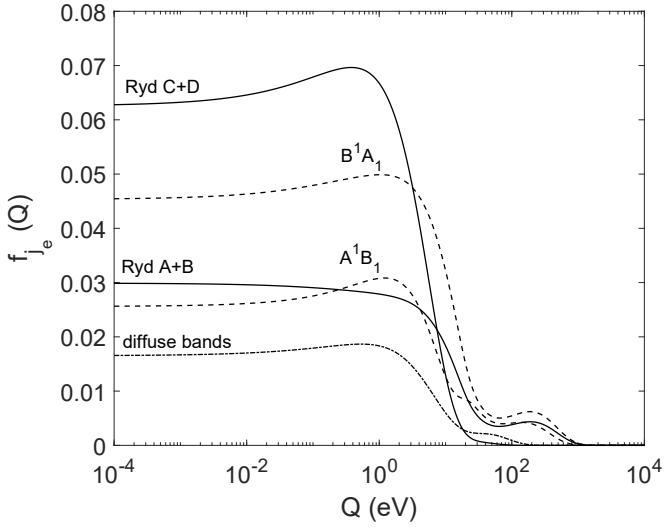

Fig. 5. Bethe sum, eq. (31), for the five excitation processes of liquid water labelled in the figure in terms of recoil energy Q.

created and implemented for protons from 100 MeV to 300 MeV. They are interpolated models, i.e. they use data tables of cross section values for each liquid water shell obtained, in this case, with RPWBA theory including Fermi density correction. Each of them were added to *G4DNAIonisation* and *G4DNAExcitation* process classes, respectively, complementary to the two lower energy models already available, thus extending the current upper limit of both existing processes (100 MeV).

With the aim of verifying the implementation of models and cross section dataset in the extended energy regime, the stopping power and range of protons were determined with the extended examples *spower* and *range* (Incerti et al., 2018), available with the Geant4 official release (v10.5). Comparison with reference data were done with the relative difference with respect to these data

$$\varepsilon(\%) = \frac{x - x_{\text{ref}}}{x_{\text{ref}}} \times 100, \tag{32}$$

where x is the value calculated with Geant4-DNA examples and x_{ref} the corresponding reference value. Stopping power and range results, compared with reference data, are shown in section 3.2.

3. Results and discussion

3.1. Comparison with Geant4-DNA dataset in the range 10–100 MeV

In order to ensure a good transition with the current model implemented in Geant4-DNA for protons below 100 MeV (the Born model (Incerti et al., 2010a)) differential and total cross section were calculated with our approach based on RPWBA theory above 10 MeV.

Fig. 6 displays differential cross sections for protons from 10 to 300 MeV obtained from calculations based on RPWBA, compared with those extracted from the Born model dataset of Geant4-DNA where possible (up to 100 MeV). For all incident energies, curves show a similar dependence with W, having similar maximum values located at similar W values; the maximum decreases with increasing incident E. This reflects the fact that the Born model in Geant4-DNA database is obtained using theoretical approaches and relativistic corrections which makes it comparable to the RPWBA theory of this work. The highest discrepancy is localized around the 21 eV peak as consequence of the difference in GOS values. Looking at Fig. 1, it can be seen that for an energy transfer $W = 10$ eV, the integration limit Q_- takes values around 10^{-3} eV for an incident energy interval from 10 to 100 MeV. Only the valence shells contribute to the DCS in the W interval from 10 to 100 eV and, as shown in Fig. 4, the valence shells GOS are roughly constant and equal to the GOS at optical limit between Q values from 10^{-3} eV–10^{0} eV. Thus the differences observed in the DCS are mostly due to differences in the optical oscillator strength (OOS) used in each model. The OOS was obtained by fitting experimental measurements of the dielectric function to a sum of Drude functions, eqs. (20) and (21), whereas the Born model was based on the data published by Heller et al. (1974), and this work was based on the data published by Hayashi et al. (2000). Further comparison and analysis can be found elsewhere (Emfietzoglou and Nikjoo, 2005).

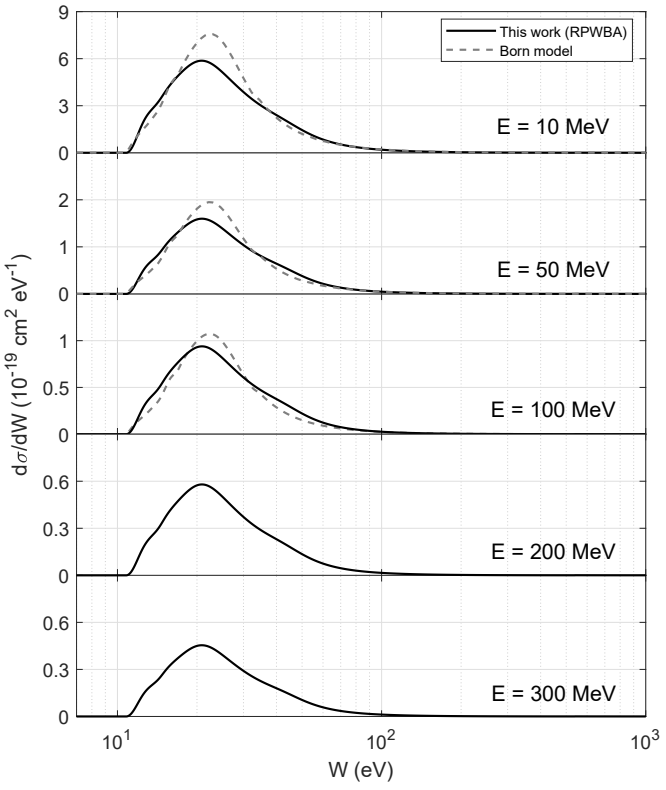

Fig. 6. Ionization differential cross section of liquid water as function of proton energy loss W for different incident energies E. Calculations with RPWBA theory (this work, solid line), and with the Born model dataset included in the Geant4-DNA database (dashed line, up to 100 MeV) are shown.

Fig. 7 shows the total cross section for ionization, summed over all shells, and the total cross section for excitation, summed also over all transitions, obtained with our model for incident energy E values from 10 to 300 MeV, and the Born model present in the Geant4-DNA database for incident energy E values from 10 to 100 MeV. Both models have the same decreasing behaviour for increasing E, noting that the Born model decreases faster both for ionization and excitation. In case of ionization, both curves intercept at 62 MeV, and our model produces a total cross section about 5% larger than that calculated with the Born model at 100 MeV. In case of excitation, the Born model produces higher values along the entire energy range studied with a relative difference with respect to this work of 2% at $E = 100$ MeV.

Since the Geant4-DNA cross section database for liquid water contains the values for each ionization shell and excitation transition separately, Table 1 shows the relative contribution to the cross section, χ, of each one calculated as

$$\chi_{j_i/j_e}(\%) = 100\ \frac{\sigma_{j_i/j_e}}{\sum_{j_i}\sigma_{j_i} + \sum_{j_e}\sigma_{j_e}}, \tag{33}$$

where j_i stands for ionization shells and j_e for excitation transitions. As stated earlier, our work and calculations based on the Born model included in the Geant4-DNA database were based on the same semi-empirical model function, but they use different experimental

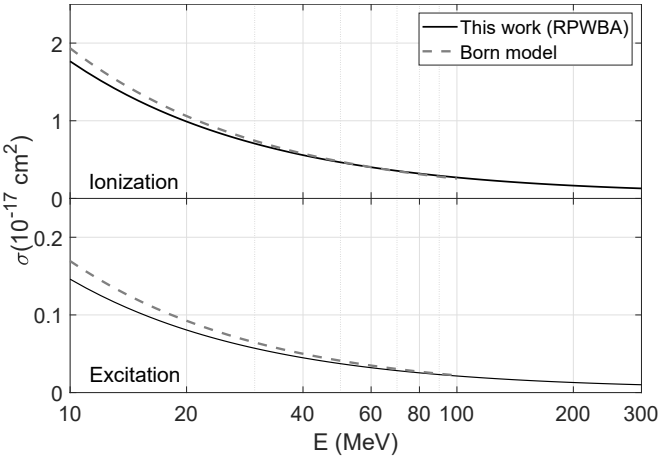

Fig. 7. Total cross section for ionization and excitation processes of liquid water as function of the proton incident energy E. The cross sections obtained with RPWBA theory (this work, solid line), and Born model dataset included in the Geant4-DNA database (dashed line, up to 100 MeV) are shown.

Table 1
Percentage of total cross section contribution for each transition, ionization and excitation processes, obtained for three different proton incident energies *E*. The calculations with RPWBA theory (this work) and with Born model dataset included in the Geant4-DNA database are listed.

		Cross section contribution (%)					
		E = 10 MeV		E = 50 MeV		E = 100 MeV	
		RPWBA	Born	RPWBA	Born	RPWBA	Born
Ionization	K-shell	0.5	0.2	0.6	0.4	0.6	0.5
	$2a_1$	14.2	5.6	14.5	5.7	14.6	5.8
	$1b_2$	20.7	23.1	21.2	23.4	21.3	23.5
	$3a_1$	22.8	30.2	22.6	30.4	22.5	30.4
	$1b_1$	34.1	32.5	33.6	32.0	33.7	31.7
Excitation	Diffuse bands	0.5	1.8	0.5	1.9	0.5	2.0
	Ryd C + D	1.9	1.5	1.9	1.5	1.9	1.6
	Ryd A + B	1.1	1.6	1.1	1.4	1.1	1.4
	B^1A_1	2.4	2.3	2.3	2.1	2.2	2.0
	A^1B_1	1.8	1.2	1.7	1.2	1.6	1.1

measurements to fit the coefficients of extended-Drude functions. There is also another difference in the way that each work truncates the extended-Drude function to reproduce the ionization threshold. The result is that the contribution of ionization shells and excitation transitions varies between both models. It is noticed an increase of the $2a_1$ shell contribution and a reduction on the $3a_1$ shell contribution of our RPWBA calculations with respect to those from the Born model. For excitation, the largest difference was found in the diffuse bands, being the contribution up to four times lower in our calculations as compared with those based on the Born model.

3.2. Validation with "spower" and "range" Geant4 examples

Fig. 8, upper panel, compares the mass stopping power calculated with the example *spower* of the Geant4 toolkit, using our implemented cross-section dataset (crosses) and the Born model dataset (empty circles), against the mass stopping power values published in the ICRU90 report (Report 90, 2014) (solid line), which were used as reference; the shaded area around ICRU90 data represents 1% uncertainty, as discussed in the ICRU90 report. Lower panel contains the relative differences calculated as stated in eq. (32). Results are in very good agreement, all deviations being lower than 1% for the extended energy range (100–300 MeV); thus, within reported uncertainties.

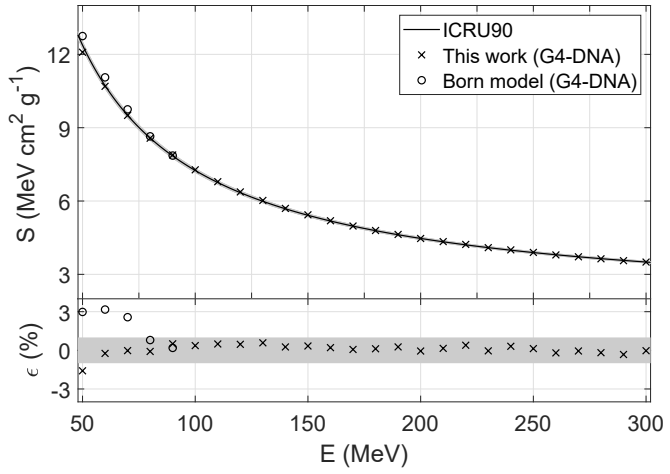

Fig. 8. Mass Stopping Power of liquid water as function of the proton incident energy *E*. The upper plot shows reference data from ICRU90 (Report 90, 2014) (solid line), mass stopping power values calculated with the Geant4-DNA *spower* example using our cross section dataset (crosses), and the Born model dataset (empty circles). Shaded area corresponds to 1% uncertainty of ICRU90 data. The lower plot shows the relative deviations with respect to ICRU90.

Fig. 9a, upper panel, shows the calculations carried out with the *range* example of the Geant4 toolkit to compare the range calculated for protons above 50 MeV against the range values published in the ICRU90 (Report 90, 2014) report for liquid water. As the calculation of range values requires the simulation of protons tracks from their initial energy down to the cutoff energy, the different models included in Geant4-DNA take part in this procedure within their respective energy range. For the new extended energy region (crosses) the Drude (0 eV–500 keV), Born (500 keV–100 MeV) and RPWBA (100–300 MeV) models are used, while for current energy regime (empty circles) only the first two contribute. Analogously to the previous example, lower panel shows the relative residuals of our Geant4-DNA calculations with respect to the ICRU90 data. Calculated values are systematically lower than reference data. The absolute difference remains roughly constant for the extended energy range ($E > 100$ MeV), being within the interval from 0.11 g cm^{-2} to 0.15 g cm^{-2}. This results in a decreasing behaviour of relative differences with increasing *E*, as shown in lower plot. Statistical uncertainties of range simulations grow proportionally to simulated range value, producing an approximately constant relative error of about 1%, represented with error bars in the plot.

To perform a test of our cross section dataset (for protons above 100 MeV) without propagating the uncertainty due to the cross sections calculated with other models below 100 MeV, we carried out other calculations with the *range* example in which proton tracking was cut at 100 MeV. Fig. 9b, upper panel, shows the calculations obtained with the proton tracking cut applied. ICRU90 range values were calculated using the continuous-slowing-down approximation (CSDA), i.e. reference data were calculated by subtracting the range for 100 MeV protons to the range at the energy specified. Calculated values are again lower than reference data, but absolute differences are now below 0.028 g cm^{-2}, which is one order of magnitude lower than the previous residuals (i.e. incorporating the calculation below 100 MeV, done with cross sections based on the Born model). Lower panel shows the relative residuals, calculated with eq. (32). The agreement observed is remarkable, being all deviations below 0.5%.

4. Conclusions

A new model for the Geant4-DNA Monte Carlo toolkit that extends the 100 MeV upper energy limit for proton interaction with liquid water (ionization and excitation processes) is presented in this paper. This work will be included in Geant4 from 11.1 beta release of the Geant4 toolkit. The model is based on the RPWBA theory using the liquid water GOS modelled with a sum of extended-Drude functions together with the Fermi density effect correction. The DCS in energy loss for ionization was calculated with RPWBA theory and compared with the existing Geant4-DNA model (the Born model) for protons at 10, 50 and 100 MeV. The largest difference was observed around the 21 eV peak, caused by the use of different experimental data for Drude function parameter

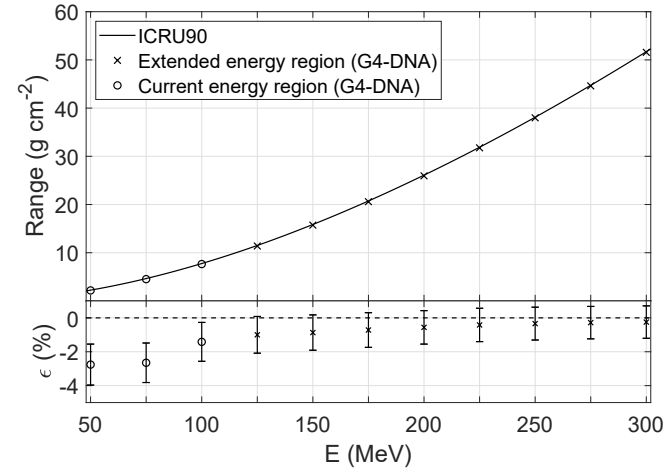

(a)

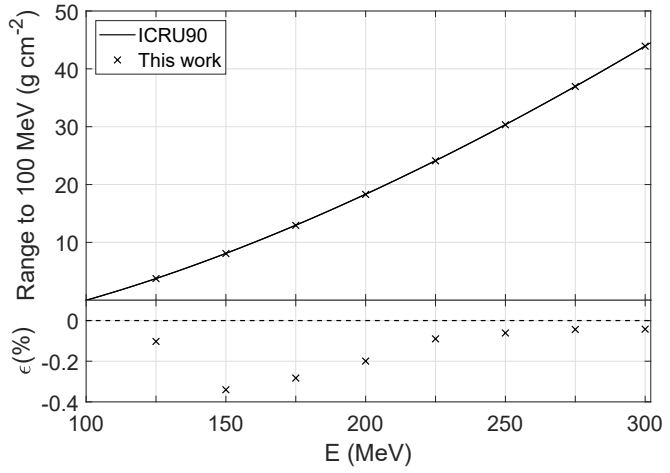

(b)

Fig. 9. (a) Mass Range of protons in liquid water as function of the incident energy *E*. The upper panel shows reference data from ICRU90 (Report 90, 2014) (solid line), mass range values calculated with the Geant4-DNA *range* example. The extended energy region (crosses, above 100 MeV) shows calculations where our model based on RPWBA was applied while the proton kinetic energy was greater than 100 MeV, whereas Born and Drude models were applied below 100 MeV. For initial energies below 100 MeV (circles), the latter are solely applied. The lower panel shows the relative difference in percentage to ICRU90. Vertical bars correspond to relative error calculated by the example code. (b) Mass Range of protons in liquid water, excluding the residual range at 100 MeV, as function of the incident energy *E*. The upper panel shows reference data from ICRU90 (Report 90, 2014) (solid line) and mass stopping power values calculated with the Geant4-DNA *range* example using our cross section dataset (empty circles). The lower panel shows the relative difference in percentage to ICRU90.

estimation. The CS for ionization and excitation were also calculated with our approximation and compared for proton incident energy from 10 to 100 MeV, with a discrepancy at 100 MeV of 5% and 2% for each process, respectively. Model validation in extended energy regime from 100 to 300 MeV was done via the comparison of stopping power and range, obtained with *spower* and *range* examples using our DCS and CS data, with ICRU90 reference data. In both cases, relative differences from reference data were below 1%. In summary, the new model presented extends the current Geant4-DNA energy limit to 300 MeV, enough to cover the entire range of proton therapy clinical beams within the accuracy reported by ICRU90 report.

Author contributions

Conceptualization, A.D.D.-M., M.I.G., Z.F., S.I. and M.A.C.-G.; Methodology, A.D.D.-M., M.I.G. and M.A.C.-G.; Software, A.D.D.-M. and M.A.C.-G.; Formal Analysis, A.D.D.-M., M.I.G. and M.A.C.-G.; Validation, A.D.D.-M and M.I.G.; Investigation, A.D.D.-M., M.I.G. and M.A.C.-G.; Resources, M.C.B, Z.F, and S.I.; Writing-Original Draft Preparation, A.D.D.-M., M.I.G. and M.A.C.-G.; Writing-Review and Editing, A.D.D.-M., M.I.G, M.C.B., Z.F, S.I and M.A.C.-G.; Visualization, A.D.D.-M., M.I.G. and M.A.C.-G.; Supervision, M.I.G. and M.A.C.-G.; Project Administration, M.I.G and M.A.C.-G.; Funding Acquisition, S.I. and M.A.C.-G.

Funding

This work received funding from Grant RTI2018-098117-B-C21 funded by MCIN/AEI/10.13039/501100011033 and by "ERDF A way of making Europe", from the Council for Innovation, Science and Commerce, Junta de Andalucía, under grant no. P18-RT-1900, cofunded by the Operational Program ERDF Andalusia 2014–2020 "Growth smart: an economy based on knowledge and innovation", and from the European Space Agency "BioRad III" contract 4000132935/21/NL/CRS. A.D.D.-M.'s contract is funded by the Spanish Ministerio de Ciencia, Innovación y Universidades under Grant No. FPU16/07020.

Declaration of competing interest

The authors declare that they have no known competing financial interests or personal relationships that could have appeared to influence the work reported in this paper.

Acknowledgments

We are grateful to Prof. Francesc Salvat for many useful discussions regarding the RPWBA theory. Monte Carlo simulations presented in this work were carried out at the FIS-ATOM computing cluster hosted at CICA (Seville, Spain).

References

Baba, K., Kusumoto, T., Okada, S., Ogawara, R., Kodaira, S., Raffy, Q., Barillon, R., Ludwig, N., Galindo, C., Peaupardin, P., Ishikawa, M., 2021a. Quantitative estimation of track segment yields of water radiolysis species under heavy ions around Bragg peak energies using Geant4-DNA. Sci. Rep. 11 (1), 1524. https://doi.org/10.1038/s41598-021-81215-6. URL. http://www.nature.com/articles/s41598-021-81215-6.

Baba, K., Kusumoto, T., Okada, S., Ishikawa, M., 2021b. A simulation-based study on water radiolysis species for 1 H + , 4 He 2+ , and 12 C 6+ ion beams with multiple ionization using Geant4-DNA. J. Appl. Phys. 129 (24), 244702 https://doi.org/10.1063/5.0054665. URL. https://aip.scitation.org/doi/10.1063/5.0054665.

Bernal, M.A., Bordage, M.C., Brown, J.M.C., Davídková, M., Delage, E., El Bitar, Z., Enger, S.A., Francis, Z., Guatelli, S., Ivanchenko, V.N., Karamitros, M., Kyriakou, I., Maigne, L., Meylan, S., Murakami, K., Okada, S., Payno, H., Perrot, Y., Petrovic, I., Pham, Q.T., Ristic-Fira, A., Sasaki, T., Štěpán, V., Tran, H.N., Villagrasa, C., Incerti, S., 2015. Track structure modeling in liquid water: a review of the Geant4-DNA very low energy extension of the Geant4 Monte Carlo simulation toolkit. Phys. Med. 31 (8), 861–874. https://doi.org/10.1016/j.ejmp.2015.10.087. URL. https://linkinghub.elsevier.com/retrieve/pii/S1120179715010042.

Bertolet, A., Baratto-Roldán, A., Barbieri, S., Baiocco, G., Carabe, A., Cortés-Giraldo, M. A., 2019a. Dose-averaged LET calculation for proton track segments using microdosimetric Monte Carlo simulations. Med. Phys. 46 (9), 4184–4192. https://doi.org/10.1002/mp.13643. URL. https://onlinelibrary.wiley.com/doi/abs/10.1002/mp.13643.

Bertolet, A., Baratto-Roldán, A., Cortés-Giraldo, M.A., Carabe-Fernandez, A., 2019b. Segment-averaged LET concept and analytical calculation from microdosimetric quantities in proton radiation therapy. Med. Phys. 46 (9), 4204–4214. https://doi.org/10.1002/mp.13673. URL. https://onlinelibrary.wiley.com/doi/abs/10.1002/mp.13673.

Dingfelder, M., 2014. Updated model for dielectric response function of liquid water. Appl. Radiat. Isot. 83, 142–147. https://doi.org/10.1016/j.apradiso.2013.01.016. URL. https://linkinghub.elsevier.com/retrieve/pii/S0969804313000171.

Dingfelder, M., Hantke, D., Inokuti, M., Paretzke, H.G., 1999. Electron inelastic-scattering cross sections in liquid water. Radiat. Phys. Chem. 53 (1), 1–18. https://doi.org/10.1016/S0969-806X(97)00317-4.

Dingfelder, M., Inokuti, M., Paretzke, H.G., 2000. Inelastic-collision cross sections of liquid water for interactions of energetic protons. Radiat. Phys. Chem. 59 (3), 255–275. https://doi.org/10.1016/S0969-806X(00)00263-2.

Emfietzoglou, D., Nikjoo, H., 2005. The effect of model approximations on single-collision distributions of low-energy electrons in liquid water. Radiat. Res. 163 (1), 98–111. https://doi.org/10.1667/RR3281. URL. http://www.bioone.org/doi/10.1667/RR3281.

Emfietzoglou, D., Cucinotta, F.A., Nikjoo, H., 2005. A complete dielectric response model for liquid water: a solution of the Bethe Ridge problem. Radiat. Res. 164 (2), 202–211. https://doi.org/10.1667/RR3399.

Emfietzoglou, D., Garcia-Molina, R., Kyriakou, I., Abril, I., Nikjoo, H., 2009. A dielectric response study of the electronic stopping power of liquid water for energetic protons and a new I-value for water. Phys. Med. Biol. 54 (11), 3451–3472. https://doi.org/10.1088/0031-9155/54/11/012.

Emfietzoglou, D., Papamichael, G., Nikjoo, H., 2017. Monte Carlo electron track structure calculations in liquid water using a new model dielectric response function. Radiat. Res. 188 (3), 355–368. https://doi.org/10.1667/RR14705.1.

Fano, U., 1963. Penetration of protons, alpha particles, and mesons. Annu. Rev. Nucl. Sci. 13 (1), 1–66. https://doi.org/10.1146/annurev.ns.13.120163.000245.

Fermi, E., 1940. The ionization loss of energy in gases and in condensed materials. Phys. Rev. 57 (6), 485–493. https://doi.org/10.1103/PhysRev.57.485.

Fernández-Varea, J.M., Salvat, F., Dingfelder, M., Liljequist, D., 2005. A relativistic optical-data model for inelastic scattering of electrons and positrons in condensed matter. Nucl. Instrum. Methods Phys. Res. Sect. B Beam Interact. Mater. Atoms 229 (2), 187–218. https://doi.org/10.1016/j.nimb.2004.12.002. URL. https://linkinghub.elsevier.com/retrieve/pii/S0168583X04012595.

Hayashi, H., Watanabe, N., Udagawa, Y., Kao, C.C., 2000. The complete optical spectrum of liquid water measured by inelastic x-ray scattering. Proc. Natl. Acad. Sci. U. S. A 97 (12), 6264–6266. https://doi.org/10.1073/pnas.110572097. URL. http://www.pnas.org/cgi/doi/10.1073/pnas.110572097.

Heller, J.M., Hamm, R.N., Birkhoff, R.D., Painter, L.R., 1974. Collective oscillation in liquid water. J. Chem. Phys. 60 (9), 3474–3482. https://doi.org/10.1063/1.1681563. URL. http://aip.scitation.org/doi/10.1063/1.1681563.

S. Heredia-Avalos, R. Garcia-Molina, J. M. Fernández-Varea, I. Abril, Calculated energy loss of swift He, Li, B, and N ions in SiO2, Al2O3, and ZrO2, Phys. Rev. A - Atom. Mol. Optic. Phys. 72 (5). doi:10.1103/PhysRevA.72.052902.

Incerti, S., Ivanchenko, A., Karamitros, M., Mantero, A., Moretto, P., Tran, H.N., Mascialino, B., Champion, C., Ivanchenko, V.N., Bernal, M.A., Francis, Z., Villagrasa, C., Baldacchino, G., Guèye, P., Capra, R., Nieminen, P., Zacharatou, C., 2010a. Comparison of GEANT4 very low energy cross section models with experimental data in water. Med. Phys. 37 (9), 4692–4708. https://doi.org/10.1118/1.3476457. URL.

Incerti, S., Baldacchino, G., Bernal, M., Capra, R., Champion, C., Francis, Z., GuÈye, P., Mantero, A., Mascialino, B., Moretto, P., Nieminen, P., Villagrasa, C., Zacharatou, C., 2010b. The Geant4-DNA project. arXiv:0910.5684 Int. J. Model. Simul. Scientif. Comput. 1 (2), 157–178. https://doi.org/10.1142/S1793962310000122. URL. https://www.worldscientific.com/doi/abs/10.1142/S1793962310000122.

Incerti, S., Kyriakou, I., Bernal, M.A., Bordage, M.C., Francis, Z., Guatelli, S., Ivanchenko, V., Karamitros, M., Lampe, N., Lee, S.B., Meylan, S., Min, C.H., Shin, W. G., Nieminen, P., Sakata, D., Tang, N., Villagrasa, C., Tran, H.N., Brown, J.M., 2018. Geant4-DNA example applications for track structure simulations in liquid water: a report from the Geant4-DNA Project. Med. Phys. 45 (8), e722–e739. https://doi.org/10.1002/mp.13048.

Inokuti, M., 1971. Inelastic collisions of fast charged particles with atoms and molecules - the Bethe theory revisited. Rev. Mod. Phys. 43 (3), 297–347. https://doi.org/10.1103/RevModPhys.43.297. URL. https://link.aps.org/doi/10.1103/RevModPhys.43.297.

Inokuti, M., Smith, D.Y., 1982. Fermi density effect on the stopping power of metallic aluminum. Phys. Rev. B 25 (1), 61–66. https://doi.org/10.1103/PhysRevB.25.61. URL. https://link.aps.org/doi/10.1103/PhysRevB.25.61.

Jackson, J.D., Fox, R.F., 1999. Classical electrodynamics. Am. J. Phys. 67 (9), 841–842. https://doi.org/10.1119/1.19136 third ed. .

Landau, L.D., Lifshitz, E.M., King, A.L., 1961. Electrodynamics of continuous media. Am. J. Phys. 29 (9), 647–648. https://doi.org/10.1119/1.1937882.

Paganetti, H. (Ed.), 2016. Proton Therapy Physics. CRC Press. https://doi.org/10.1201/9780367803551. URL. https://www.taylorfrancis.com/books/9781439836453.

Perales, Á., Baratto-Roldán, A., Kimstrand, P., Cortés-Giraldo, M.A., Carabe, A., 2019. Parameterising microdosimetric distributions of mono-energetic proton beams for fast estimates of yD and y*. Biomed. Phys. Eng. Express 5 (4), 045014. https://doi.org/10.1088/2057-1976/ab236a. URL. https://iopscience.iop.org/article/10.1088/2057-1976/ab236a.

Report 90. NP.2–NP J. ICRU 14 (1), 2014. https://doi.org/10.1093/jicru/ndw043. URL. https://academic.oup.com/jicru/article-lookup/doi/10.1093/jicru/ndw043.

Ritchie, R.H., Hamm, R.N., Turner, J.E., Wright, H.A., Bolch, W.E., 1991. Radiation interactions and energy transport in the condensed phase. In: Physical and Chemical Mechanisms in Molecular Radiation Biology. Springer US, Boston, MA, pp. 99–135. https://doi.org/10.1007/978-1-4684-7627-9_4. URL. http://link.springer.com/10.1007/978-1-4684-7627-9_4.

Sakata, D., Lampe, N., Karamitros, M., Kyriakou, I., Belov, O., Bernal, M.A., Bolst, D., Bordage, M.-C., Breton, V., Brown, J.M., Francis, Z., Ivanchenko, V., Meylan, S., Murakami, K., Okada, S., Petrovic, I., Ristic-Fira, A., Santin, G., Sarramia, D., Sasaki, T., Shin, W.-G., Tang, N., Tran, H.N., Villagrasa, C., Emfietzoglou, D., Nieminen, P., Guatelli, S., Incerti, S., 2019. Evaluation of early radiation DNA damage in a fractal cell nucleus model using Geant4-DNA. Phys. Med. 62, 152–157. https://doi.org/10.1016/j.ejmp.2019.04.010. URL. https://linkinghub.elsevier.com/retrieve/pii/S1120179719300882.

Salvat, F., 2013. A generic algorithm for Monte Carlo simulation of proton transport. Nucl. Instrum. Methods Phys. Res. Sect. B Beam Interact. Mater. Atoms 316, 144–159. https://doi.org/10.1016/j.nimb.2013.08.035. URL. https://linkinghub.elsevier.com/retrieve/pii/S0168583X13009191.

Scifoni, E., Surdutovich, E., Solov'yov, A.V., 2010. Spectra of secondary electrons generated in water by energetic ions. Phys. Rev. 81 (2), 021903 https://doi.org/10.1103/PhysRevE.81.021903. URL. https://link.aps.org/doi/10.1103/PhysRevE.81.021903.

Shin, W.-G., Ramos-Mendez, J., Tran, N.H., Okada, S., Perrot, Y., Villagrasa, C., Incerti, S., 2021. Geant4-DNA simulation of the pre-chemical stage of water radiolysis and its impact on initial radiochemical yields. Phys. Med. 88, 86–90. https://doi.org/10.1016/j.ejmp.2021.05.029. URL. https://linkinghub.elsevier.com/retrieve/pii/S1120179721002118.

Sternheimer, R.M., Seltzer, S.M., Berger, M.J., 1982. Density effect for the ionization loss of charged particles in various substances. Phys. Rev. B 26 (11), 6067–6076. https://doi.org/10.1103/PhysRevB.26.6067.